Biofabrication

CrossMark

Improving alginate printability for biofabrication: establishment of a universal and homogeneous pre-crosslinking technique

Jonas Hazur[1] , Rainer Detsch[1], Emine Karakaya[1], Joachim Kaschta[2], Jörg Teßmar[3], Dominik Schneidereit[4], Oliver Friedrich[4], Dirk W Schubert[2] and Aldo R Boccaccini[1,5]

1   Institute of Biomaterials, University of Erlangen-Nuremberg, Cauerstr.6, 91058, Erlangen, Germany
2   Institute for Polymer Materials, University of Erlangen-Nuremberg, Martensstraße 7, 91058, Erlangen, Germany
3   Department for Functional Materials in Medicine and Dentistry, University of Würzburg, Pleicherwall 2, 97070, Würzburg, Germany
4   Institute of Medical Biotechnology, University of Erlangen-Nuremberg, Paul-Gordan-Str. 3, 91052, Erlangen, Germany

E-mail: aldo.boccaccini@fau.de

Abstract

Many different biofabrication approaches as well as a variety of bioinks have been developed by researchers working in the field of tissue engineering. A main challenge for bioinks often remains the difficulty to achieve shape fidelity after printing. In order to overcome this issue, a homogeneous pre-crosslinking technique, which is universally applicable to all alginate-based materials, was developed. In this study, the Young's Modulus after post-crosslinking of selected hydrogels, as well as the chemical characterization of alginate in terms of M/G ratio and molecular weight, were determined. With our technique it was possible to markedly enhance the printability of a 2% (w/v) alginate solution, without using a higher polymer content, fillers or support structures. 3D porous scaffolds with a height of around 5 mm were printed. Furthermore, the rheological behavior of different pre-crosslinking degrees was studied. Shear forces on cells as well as the flow profile of the bioink inside the printing nozzle during the process were estimated. A high cell viability of printed NIH/3T3 cells embedded in the novel bioink of more than 85% over a time period of two weeks could be observed.

1. Introduction

The fields of regenerative medicine, cell therapy and tissue engineering (TE) have been growing constantly in recent years. Especially in soft tissue engineering approaches, naturally occurring polymeric materials are used to create scaffolds, as they often show biocompatibility and suitable biodegradability [1]. Moreover, their features to mimic the native extracellular matrix due to their hydrophilicity, high water content and physical characteristics, render them suitable as matrix for biofabrication approaches [2].

In this study, we used alginate as a base material for the development of bioinks; a material that has been broadly characterized in literature [3–12]. Alginate based bioinks are commonly used for dispense plotting, which requires to join various property requirements at once [13, 14]. Li *et al* have

summarized those requirements and divided them into two main categories: Properties of bioink vs. properties of constructs. Those categories can be then further divided into rheological properties, adhesion between layers, shape fidelity, cell viability and degradability [15].

In order to adapt the mechanical properties and printability of alginate based bioinks, mostly (1) multi-material bioinks [16–19], (2) non-degradable particle or fiber filled systems [20–23] or (3) printing with support (sacrificial) material [24, 25] are utilized. All those approaches have the common goal of overcoming the lack of shape fidelity of pure alginate solutions, which is due to the mostly viscous characteristics dominating over the elastic behavior of non-crosslinked polymer solutions. Although these methods work well, in general they also face certain challenges. When using multi-material bioinks for example, the solid content of those hydrogels often exceeds 10% (w/v) or the bioinks are still deficient

5   Author to whom any correspondence should be addressed.

in terms of printability. The drawback of such high polymer concentrations is that the mesh size of the polymer network decreases, resulting in significant barriers to diffusive transport of soluble factors and nutrients [26–28]. Moreover, in case of non- or comparably slow degrading fillers the question arises, whether residual filler particles will lead to interactions with the surrounding tissue, once the matrix is degraded. When considering sacrificial support materials, depending on the size of the printed structure, it can be challenging to remove all of the support material sufficiently. Furthermore, usually one additional step after crosslinking has to be conducted. Moreover, the 3rd dimension, meaning the actual height of the printed constructs, is often not shown or specified. Thus, in our approach, we aimed to design an alginate-based bioink with low polymer content which is capable to form high volume, porous, cell-laden 3D structures without deploying a second matrix material, thickeners, non-degradable fillers or sacrificial support materials.

In order to achieve this goal, we had the intention to create a loosely pre-crosslinked alginate network, giving just enough stability to preserve its shape after printing. Apart from this, an important aspect of such a bioink is its homogeneity. This is why a homogeneous pre-crosslinking technique, which is universally applicable to all alginate-based bioinks was developed, combining the following ideas. On the one hand, it could already be shown, that CaCl$_2$ pre-crosslinked alginate bioinks can be applied for bioprinting [29, 30]. However, due to the rapid reaction of free Ca^{2+}-ions with alginate, it is very difficult to achieve homogeneously crosslinked hydrogels and thus also bioinks [31]. Marchioli *et al* [29] for example reported viscosity data of their CaCl$_2$ pre-crosslinked bioink with a marked standard deviation ($\eta = 2923.33 \pm 958.45$ Pas) and found it to be non-suitable for bioprinting compared to other bioinks prepared in their work. Furthermore, Chung *et al* [32] and Paxton *et al* [30] reported printing of 3–4 layered scaffolds with CaCl$_2$ pre-crosslinked alginate hydrogels, but the images reveal rather uneven, inhomogeneous strands. On the other hand, an internal gelation method has been used previously in order to create homogeneously crosslinked alginate structures. In comparison to external gelation, where ions are first crosslinking the structure on the surface and then diffusing into the bulk, ions are released all over the bulk structure during internal gelation. All such structures were shaped by mold casting or membrane emulsification [5, 33–35]. In order to control the crosslinking kinetics and thus, to produce more homogeneous bioinks, the internal gelation method was chosen in the current study for pre-crosslinking. Figure 1 illustrates the application of pre-crosslinked alginate bioinks schematically and gives an overview of the appropriated volume ratios during preparation, as well as the processing parameters.

2. Materials and methods

2.1. Chemical characterization of alginate

Sodium alginate powder (VIVAPHARM® alginate PH176) from brown algae, with approval as pharmaceutical excipient, was purchased from JRS PHARMA GmbH & Co. KG (Rosenberg, Germany). The particle size distribution is declared between 150–200 μm, whereas the viscosity of a 1% (w/v) solution of the sodium salt lies in the range of 550–750 mPas, according to the supplier.

2.1.1. Chain composition.

In order to investigate the M/G ratio of alginate, a reduction of the molecular weight by partial hydrolysis was performed, according to Jensen *et al* [36]. Firstly, 100 mg of alginate were dispersed in 2 ml ethanol and dissolved in 100 ml H$_2$O. After adjusting the pH to 5.6 by adding HCl the solution was refluxed at 100 °C for 1 h. Subsequently, the pH was decreased to 3.8 by addition of HCl and refluxed for further 20 min. After cooling down to 0 °C, NaOH was used to finally neutralize the solution. ^{1}H nuclear magnetic resonance (NMR) spectra of 5 mg lyophilized alginate sample in 0.5 ml D$_2$O were recorded on a Bruker Advance 500 spectrometer (Bruker Biospin, GmbH, Rheinstettem, Germany) operating at 400 MHz. In order to obtain the M/G ratio, the relative integrals of the three signals in the anomeric region were calculated which contain specific information about the chain composition. Signals of the region A, B and C according to Jensen *et al* were integrated and the M/G ratio could be determined with the equation deduced by Grasdalen (equation (5)) [37]:

$$M/G = \frac{(I_B + I_C - I_A)}{I_A} \qquad (5)$$

2.1.2. Determination of molecular weight

Gel permeation chromatography (GPC) was performed, using a GPC Max TDA 305 (Malvern Instruments Ltd., Worcestershire, UK). For the measurements a water system with a flow rate of 0.7 ml min^{-1} and an injection Volume of 100 μl with a set of single-pore polymethyl-methacrylate columns (A2000 & A3000, Malvern Instruments Ltd., Worcestershire, UK) was used. The detector and column temperature were kept constant at 35 °C and 0.1 M NaNO$_3$ solution was used as solvent.

2.2. Ink formation
2.2.1. Alginate solutions

Alginate solutions were prepared by dissolving sodium alginate powder in Dulbecco's Phosphate Buffered Saline without Calcium and Magnesium (DPBS, no calcium, no magnesium, Gibco^{TM}—Thermo Fisher Scientific, Massachusetts, USA). To ensure complete dissolution of alginate, the solutions were stirred for at least 12 h at room temperature and
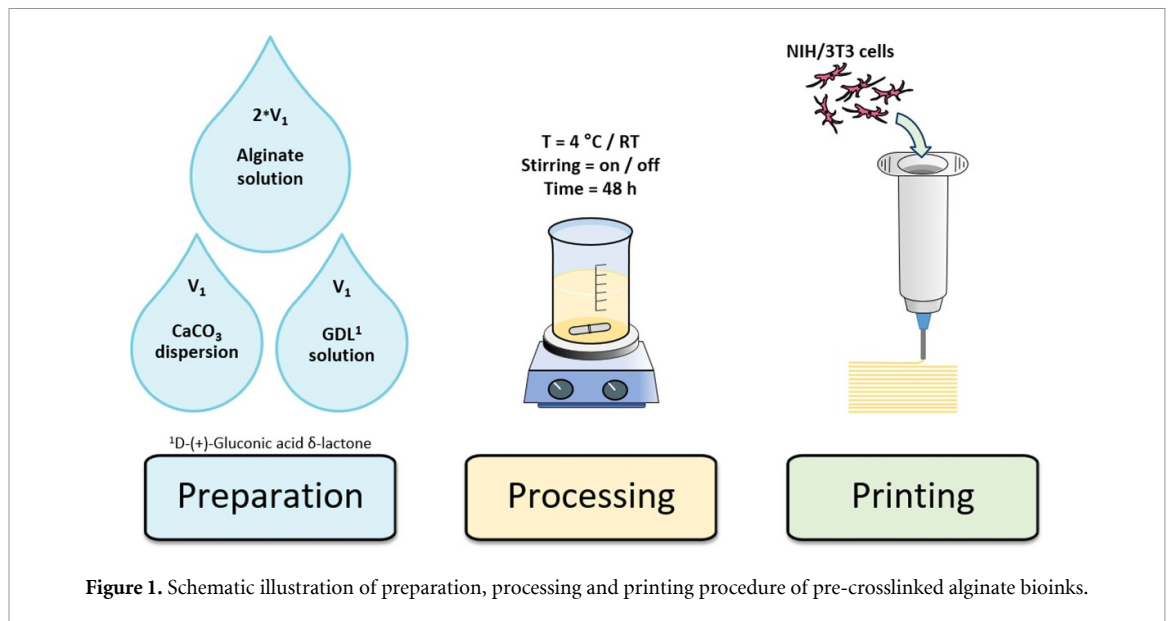
Figure 1. Schematic illustration of preparation, processing and printing procedure of pre-crosslinked alginate bioinks.

the containers were additionally sealed with PARA-FILM® (Pecheney Plastics Packaging, Chicago, USA), to prevent solvent evaporation. The alginate concentration was set to 2% (w/v).

2.2.2. Pre-crosslinked alginate hydrogels

In order to fabricate pre-crosslinked alginate hydrogels for bioprinting, first alginate solutions with a concentration of 4% (w/v) were prepared as described in section 2.2.1. Subsequently, $CaCO_3$ (Calcium carbonate precipitated for analysis EMSURE®, CAS 471-34-1, Merck KGaA, Darmstadt, Germany) and D-Glucono-δ-lactone (CAS 90-80-2, Merck KGaA, Darmstadt, Germany) were mixed with ultrapure water type 1 separately and then slowly added to the alginate solution while stirring. $CaCO_3$ dispersions were added first and D-Glucono-δ-lactone (GDL) solutions were afterwards added dropwise, using a micro-pipette. GDL was chosen, as it is already used in some medical products, where it serves as irrigation solution to prevent clogs in bladder catheters and is applied for hydrofluoric acid burn management in the form of calcium gluconate gels [38, 39]. The initial concentrations of $CaCO_3$ dispersions were 20, 50 and 80 mM and corresponding GDL solutions always had twice the concentration (40, 100 and 160 mM respectively), leading to the final values seen in table 1. This ratio was on the one hand chosen for all experiments due to the fact that $CaCO_3$ needs two protons to dissolve. On the other hand, GDL will undergo hydrolysis when dissolved in water to form gluconic acid, which then has one carboxylic acid group to release one proton [40, 41]. Thus, in theory this ratio would serve to exactly dissolve the $CaCO_3$ particles, without further decrease of the pH. Preliminary results also showed that around 4 mM of $CaCO_3$ particles remain undissolved. However, $CaCO_3$ particles were already shown to be resorbable

in scaffolds by MSCs as well as osteoclasts and are not suspected to have a negative influence on other cell types [42, 43]. The volume ratio between alginate-, $CaCO_3$- and GDL-solutions/dispersions was kept constant at 2:1:1, resulting in concentrations in the prepared bioinks, according to table 1. This table also serves to show the labeling system of the different bioinks analyzed in this work, including their different compositions and crosslinking environments. During the gelation time of two days, the hydrogel was either kept at room temperature or in a temperature-controlled room at 4 °C, with and without stirring.

2.2.3 3D printing

For 3D-printing, a BioScaffolder 2.1 (GeSIM, Radeberg, Germany) and polypropylene needles with a stainless-steel cannula with an inner diameter of 410 μm (All-purpose dispensing tips 7 018 272, Nordson EFD, Apex Business Centre Boscombe Road Dunstable, Bedfordshire, England) were used. With this setup, squared structures with a side length of 15 mm were printed at a pressure of 17 kPa, regulated by the F-Box and a print velocity of 4 mm s^{-1}.

2.2.4. Post-crosslinking

In order to fully solidify the 3D-printed structures, a post-crosslinking step was performed. In this step, the alginate hydrogels were slowly covered with $CaCl_2$ (Calcium chloride dihydrate, CAS 10 035-04-8, Merck KGaA, Darmstadt, Germany) solution of 100 mM concentration and left to crosslink for 10 min. Afterwards, the $CaCl_2$-solution was removed and replaced by DPBS or Dulbecco's Modified Eagle Medium and additions (further specified in section 2.6) in the case of cell culture studies.

Table 1. Final composition and crosslinking environment of pre-crosslinked bioinks and their resulting labels.

Label	Alginate (% w/v)	$CaCO_3$ (mM)	GDL (mM)	Reaction temperature	Stirred
Alg_0mM_RT	2	0	0	RT	Yes
Alg_5mM_4 °C	2	5	10	4 °C	Yes
Alg_12.5mM_4 °C	2	12.5	25	4 °C	Yes
Alg_20mM_4 °C	2	20	40	4 °C	Yes
Alg_12.5mM_RT	2	12.5	25	RT	Yes
Alg_12.5mM_4 °C_w/o stirring	2	12.5	25	4 °C	No

2.3. Rheological evaluations

For rotational rheology measurements, an AR-G2 (AR-G2 Magnetic Bearing Rheometer, TA-Instruments Ltd., New Castle, Delaware, USA) was used. All materials described in sections 2.2.1 and 2.2.2 were tested without cells and additionally, NIH/3T3 cells were embedded into Alg_20mM_4 °C and Alg_0mM_RT bioinks and evaluated according to the following description.

In order to characterize the samples, a cross-hatched plate on plate geometry was chosen (Top: PLATE SST ST X-HATCH 40MM SMART-SWAP, serial number: 996602; Bottom: PLATE SST EHP 40MM X-HATCH SCREW-IN, TA Instruments Ltd, New Castle, Delaware, USA), with the idea to prevent slippage at the specimen geometry interface during the measurements. All solutions and hydrogels were rheologically investigated before the post-crosslinking step. For this purpose, the respective test samples were filled into a syringe, dispensed on the bottom plate geometry and finally trimmed, once the upper geometry was in place. Additionally, the upper geometries' trough was filled with distilled water and a solvent trap covered the upper and lower geometries during the measurements to avoid solvent evaporation. Each experiment was conducted three times and the arithmetic mean as well as the standard deviation (SD) were calculated. At a gap width of 0.5 mm with a pre conditioning step (120 s; 20 °C; no strain), all samples were examined with three different methods: oscillation amplitude sweep (20 °C; 10 rad*s^{-1} frequency; 0.1%–500% strain), oscillation frequency sweep (20 °C; 0.25–100 rad*s^{-1} frequency; 1.0% strain), and flow sweep (20 °C, 0.8–1000 s^{-1} shear rate). The measurements were performed using direct-strain control in either continuous rotation or oscillation mode.

The measurements were chosen based on the work of Paxton *et al* [30], but adapted to the current parameters. For analyzing the viscosity data in dependence of shear rate, either the Carreau-Yasuda or power-law model were used [44, 45]. These models and the importance in the field of biofabrication were comprehensively discussed by the group of Akhilesh K. Gaharwar [46, 47], also pointing out their limitations as well as alternative models. With those models, the velocity, residence time, shear rate and shear stress profiles in the tip could then be calculated.

2.4. Printability and shrinkage

In order to evaluate the different alginate hydrogels in terms of printability and shrinkage, an evaluation strategy was created. Images of the hydrogels were taken directly after printing with a Sony NEX-5 digital system camera and after post-crosslinking with a Stereolupe Stemi 508 light microscope. By using Fiji ImageJ software version 1.51 n, the size of all 3D printed structures was quantified [48]. Here, either the scale bar or the diameter of the well plate of 37 mm were used to set a scale in pixels/mm for microscope and digital camera images, respectively. In the images, the printed structures in cuboid shape, were overlaid with a grid of six by six lines in order to allow consistent length measurements. The arithmetic means of those measurements are indicated with an overline.

To calculate the shrinkage $\bar{S}$ of the hydrogels during post-crosslinking, the arithmetic means of the shrinkage $\bar{S}_x$ (x-direction) and $\bar{S}_y$ (y-direction), were averaged. $\bar{S}_x$ and $\bar{S}_y$ can be calculated by subtracting the averaged side length in the respective direction, before ($\bar{L}_{bx}$ and $\bar{L}_{by}$) and after ($\bar{L}_{ax}$ and $\bar{L}_{ay}$) post-crosslinking from each other, setting them in relation with the corresponding length before post-crosslinking and multiplying them by 100 %:

$$\bar{S} = \frac{\bar{S}_x + \bar{S}_y}{2} = \frac{\left(\frac{\bar{L}_{bx}-\bar{L}_{ax}}{\bar{L}_{bx}} * 100\%\right) + \left(\frac{\bar{L}_{by}-\bar{L}_{ay}}{\bar{L}_{by}} * 100\%\right)}{2}$$ (1)

Additionally, a general evaluation system for the printability of pre-crosslinked hydrogels was introduced. Here, two main aspects were considered. On the one hand, the aspect of size and on the other hand, the edge sharpness were addressed. This could be achieved by calculating a value P for printability in the range of $0 < P \leq 1$, according to equation (2):

$$P = \frac{1}{\left[\left|\frac{1}{2} * \left(\frac{\bar{L}_{bx}}{L_{0x}} + \frac{\bar{L}_{by}}{L_{0y}}\right) - 1\right| + 1\right] * \left[1 + \frac{1}{2} * \left(\frac{SD_{bx}}{L_{0x}} + \frac{SD_{by}}{L_{0y}}\right)\right]}$$ (2)

L_{0x} and L_{0y} are the provided side lengths to the printing system (in this case 15 mm), $\bar{L}_{bx}$ and $\bar{L}_{by}$ the arithmetic means and SD_{bx} and SD_{by} the standard deviations of the length measurements before post-crosslinking in x- and y-direction, respectively. As the squared structures were kept the same throughout this work, the printability P is only dependent on $\bar{L}_{bx}$, $\bar{L}_{by}$, SD_{bx} and SD_{by}. Those values can therefore be assigned to the observed size ($\bar{L}_{bx}$ and $\bar{L}_{by}$) and to

the sharpness of the contour (SD_{bx} and SD_{by}), respectively.

2.6. Nanoindentation

A Piuma Nanoindenter (Optics11, Amsterdam, Netherlands) was used for mechanical testing of the hydrogels to examine the effective Young's modulus (E_{eff}). For all measurements a boro-silicate glass tip featuring 0.46 N m^{-1} stiffness and 61 μm radius (Optics11, Amsterdam, Netherlands) was mounted to the Nanoindenter. The samples were casted, crosslinked (10 min in 0.1 M CaCl$_2$ solution) and measured in plastic petri dishes right after crosslinking (SARSTEDT AG & Co. KG, Nürnmbrecht, Germany). Hanks' Balanced Salt solution (HBSS, Sigma-Aldrich Chemie GmbH, Taufkirchen, Germany) was added on top of the samples in order to prevent desiccation of the hydrogels during the measurements. A total number of at least 22 indentations were performed for each material and equation (3) [49] was applied:

$$\frac{1}{E_{eff}} = \frac{1 - \nu^2}{E} + \frac{1 - \nu_i^2}{E_i} \quad (3)$$

where E_{eff} is the measured effective Young's Modulus of the sample, E is the real Young's Modulus of the sample, E_i the Young's Modulus of the indenter tip, ν the Poisson ratio of the sample and ν_i the Poisson ratio of the indenter tip. With the assumption, that $E_i \gg (1 - \nu_i)$, the last term of equation (3) can be neglected. For our calculations, the Poisson ratio of all hydrogels was given an estimated value of 0.5, which leads to the following correction factor to calculate the Young's Modulus:

$$E = E_{eff} * 0.75 \quad (4)$$

2.7. In vitro studies

NIH/3T3 cells (ATCC® CRL-1658™) were cultured in T-75 tissue culture flasks (TC-flask T75, Sarstedt AG & Co. KG, Nümbrecht, Germany) in Dulbecco's Modified Eagle's Medium (DMEM, high glucose, pyruvate, Gibco™—Thermo Fisher Scientific, Massachusetts, USA) with additional 10% (v/v) bovine calf serum (BCS, Sigma-Aldrich Chemie GmbH, Taufkirchen, Germany) as well as 1% (v/v) Penicillin Streptomycin (PS, Gibco™—Thermo Fisher Scientific, Massachusetts, USA), 1 mM Sodium pyruvate (100 mM Sodium pyruvate solution, Sigma-Aldrich Chemie GmbH, Taufkirchen, Germany) and additional 4 mM L-Glutamine (200 mM L-Glutamine solution, Sigma-Aldrich Chemie GmbH, Taufkirchen, Germany) at 37.5 °C and 5% CO$_2$. The cells were detached at passage 17 and counted with a Lobauer counting chamber (Neubauer-improved, Paul Marienfeld GmbH & Co.KG, Lauda König-shofen, Germany). In order to concentrate the cells

in cell culture medium to a total number of 11 Mio. cells/ml, they were centrifuged for three minutes at 500 rpm and the supernatant was discarded. After that, cells were resuspended in the medium. In order to prepare the bioinks, the initial inks were prepared under sterile conditions and allowed to reach room temperature before mixing. Those inks were filled into a syringe and subsequently mixed with the concentrated cell suspension by connecting the two syringe openings and carefully pushing the material back and forth several (at least five) times, to ensure homogeneity of the cell mixture. A volume ratio of ten to one (ink to cell suspension) was chosen, in order to achieve a final cell concentration in the bioinks of 1 Mio cells/ml. After printing (section 2.2.3) and post-crosslinking (section 2.2.4) the cell viability was evaluated with live and dead staining, using Calcein, AM (Thermo Fisher Scientific, Massachusetts, USA) and Propidium Iodide (1.0 mg ml^{-1}, Thermo Fisher Scientific, Massachusetts, USA), respectively. Triplicates of each sample after one, three, seven and 14 d were used, and each sample was imaged in five different locations. Live and dead cells were then counted in all 15 images and set in proportion to determine the cell viability. For counting, the ITCN plugin for Fiji ImageJ Version 1.51 n was used.

3D image stacks were acquired using an upright multiphoton microscopy setup (Schneidereit *et al* 2018), applying 810 nm excitation while acquiring DAPI fluorescence at 450/30 nm (ET450/30 m) and Rhodamine-Phalloidin at 620/60 nm (ET620/60 m) through an HC Fluotar L16x/0.6 CORR VISIR objective [50]. The excitation light power was 150 mW on average, the intensity was attenuated according to an exponential function in correlation to the penetration depth starting with 100 mW at the sample surface and ending at about 250 mW for the deepest image slice, to compensate for light scattering and absorption in the sample and keep fluorescence emission intensity constant over sample depth. Recording was performed with a typical voxel size of $0.4 \times 0.4 \times 1$ μm and a field of view of 600×600 μm. The images were only taken with well printable samples including NIH/3T3 cells after 14 d of cell culture, to visualize the difference of cell morphology deep inside the sample and close to the surface, as 2D images did not give enough information on this issue.

2.8. Statistical analysis

For the evaluation of Nanoindentation, at least 22 measurements were performed, and one-way ANOVA was used in order to find statistically significant differences on the 0.005 level. In contrast to that, the population variances of cell viability tests were significantly different on the 0.05 level according to Levene's Test. Due to this, a non-parametric Friedman ANOVA was performed in this case.

3. Results and discussion

As the method used in this paper utilizes $CaCO_3$ particles as inactive Ca^{2+} source, those particles can be distributed in any alginate-based solution without leading to a crosslinking reaction. By adding D-Glucono-δ-lactone (GDL), the mixture is acidified in a slow manner, leading to the dissolution of $CaCO_3$-particles and consequently crosslinking of the alginate solution, as previously reported [5, 33, 34]. In order to evaluate most requirements of bioinks [15], rheological measurements, printability studies, as well as cell viability tests were performed. In contrast to our first hypothesis that protons released by gluconic acid and used by $CaCO_3$ for dissolution should compensate one another and thus not decrease the pH level, a decrease of pH in the range from 4.96–6.05 after pre-crosslinking could be determined. The initial values of pH lay between 7.39–7.50 before pre-crosslinking. A more detailed trend of the pH level over a time period of 21 h for one specific hydrogel during pre-crosslinking can be found in section 5.3 (supplementary material). Due to the addition of a volume fraction of 1:10 of DMEM buffer solution to the bioink when cells are added, the pH increases to a value of around 6.2. After a maximum of one hour at this pH, printing was completed, followed by the crosslinking step which had no significant effect on pH. Finally, the hydrogel samples were covered with cell culture medium, which potentially leads to a further gradual increase of pH, to a value of 7.4, over time. Kruse *et al* showed that after up to 5 d at pH 6.5, cell viability of fibroblasts was above 70% [51]. The short-term effects are assumed to be significantly lower, but the shortest time period covered by Kruse *et al* was one day. Additionally, Geum-Hwa Lee *et al* observed similar results for MG63 osteoblast cell line, but covered shorter time frames down to 12 h, where cell viability was shown to be around 85% at pH 6.4 [52]. Thus, we considered that a pH level of around 6.2 affecting the cells for one hour did not decrease cell viability markedly. In addition, the potential precipitation of calcium phosphate particulates is discussed in section 5.4 (supplementary material) and it is concluded that no relevant amount of calcium phosphate is precipitated. Through GPC analysis a weight average molecular weight (M_w) of around 250 kg mol^{-1} could be determined for alginate. Moreover, NMR spectroscopy revealed a mannuronic (≈ 54 %) to guluronic acid (≈ 46 %) ratio of 1.19.
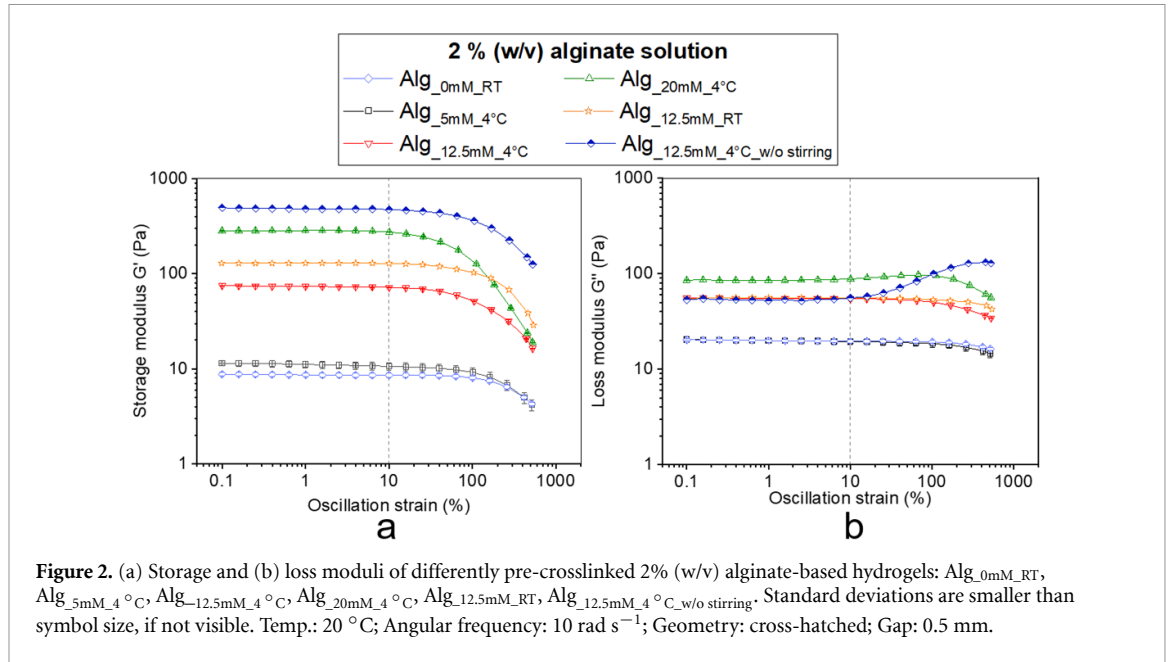
3.1. Rheology

3.1.1. Strain amplitude sweeps

With the help of amplitude sweeps, the linear viscoelastic regions of alginate hydrogels and solutions were determined and are shown in figure 2. Below strains of approximately 10% all investigated inks behave linearly viscoelastic. Thus, the amplitude for frequency sweeps was chosen to be 1.0 %, one order of magnitude below this value. Moreover, the difference in storage and loss moduli for varying parameters is shown. It can be observed that the loss moduli within the linear viscoelastic region are only dependent on the amount of $CaCO_3$ used for the pre-crosslinking and are rising with increasing amount of the latter.

In contrast to that, storage moduli are not only dependent on the amount of $CaCO_3$ used, but also on the applied preparation and conditions. Similar to the behavior of loss moduli, the storage moduli increase with the amount of $CaCO_3$, as expected. The increasing number of physical Ca^{2+} crosslinks in the hydrogels at growing $CaCO_3$ concentrations is thought to be responsible for the growing elastic response. When comparing the different methods of crosslinking at a total $CaCO_3$ concentration of 12.5 mM, it can be noticed that crosslinking at room temperature, as compared to crosslinking at 4 °C, leads to a slightly increased elastic behavior. Moreover, fabricating a pre-crosslinked alginate hydrogel with a concentration of 12.5 mM $CaCO_3$, but without stirring during the crosslinking process, increases the elastic behavior markedly, even exceeding the storage modulus of hydrogels with 20 mM total $CaCO_3$ concentration. In this case, too, it is supposed that the network formation plays the most important role for the change in the elastic behavior. When the hydrogels are not stirred during the pre-crosslinking process, there is no obstruction to the crosslinking mechanism. Thus, a hydrogel with a completely interconnected 3D structure will form. Compared to this, under the condition of stirring, an overall 3D network formation is hindered, leading to less elastic, i.e. more viscous, behavior. Moreover, it was observed that at higher temperatures the main proportion of material transition from solution to hydrogel (=network formation) occurs within a shorter period of time (section 5.3, supplementary information (available online at stacks.iop.org/BF/12/045004/mmedia)). It is assumed that with a smaller timeframe of crosslinking (e.g. RT), the alginate will be able to generate a stronger connected network, as the ratio between competing mechanisms of crosslinking (influenced by temperature; results in ↑G') and shearing (influenced by stirring; results in ↓G') is shifted. Due to this interplay, we hypothesize that G' of Alg$_{12.5mM\_4\,°C}$ will not reach the one of Alg$_{12.5mM\_RT}$ when stirred for a prolonged time. An increase in loss moduli at high oscillation amplitudes can be noticed for inks Alg$_{20mM\_4\,°C}$ and Alg$_{12.5mM\_4\,°C\_w/o\ stirring}$. In conformity with this observation, those two inks are also the ones which have the highest storage moduli. Thus, the growing amount of dissipated energy at high strains could either be explained by ripping off the strong network or by slippage at the geometry surface due to stiffer gels [53].

Figure 2. (a) Storage and (b) loss moduli of differently pre-crosslinked 2% (w/v) alginate-based hydrogels: Alg_{0mM_RT}, $Alg_{5mM\_4\,°C}$, $Alg_{12.5mM\_4\,°C}$, $Alg_{20mM\_4\,°C}$, $Alg_{12.5mM\_RT}$, $Alg_{12.5mM\_4\,°C\_w/o\,stirring}$. Standard deviations are smaller than symbol size, if not visible. Temp.: 20 °C; Angular frequency: 10 rad s^{-1}; Geometry: cross-hatched; Gap: 0.5 mm.

3.1.2. Oscillation frequency and shear flow sweeps

Additionally to amplitude sweeps, frequency sweeps and shear flow sweeps were conducted with all hydrogels, according to section 2.3. Figure 3 shows the values of viscosity η in dependence of the shear rate (flow sweep), as well as the tangent of the loss angle δ (frequency sweep).

Firstly, and most importantly, it can be observed, that all samples in figure 3(a) show shear thinning behavior, although different characteristics of the graphs can be observed. Characteristic for non-crosslinked polymer solutions, the pure alginate solution (Alg_{0mM_RT}) shows a Newtonian plateau region at low shear rates, and shear thinning behavior at high shear rates. This trend is often described with a Carreau-Yasuda or Cross-Model in literature [44]. However, those models are not suitable for crosslinked polymer-networks ($Alg_{5mM\_4\,°C}$, $Alg_{12.5mM\_4\,°C}$, $Alg_{20mM\_4\,°C}$, $Alg_{12.5mM\_RT}$ and $Alg_{12.5mM\_4\,°C\_w/o\,stirring}$). In case of crosslinking with the lowest amount of crosslinking agent ($Alg_{5mM\_4\,°C}$), the trend of the curve in figure 3(a) is still comparable to the non-crosslinked alginate solution (Alg_{0mM_RT}). The main difference is that at low shear rates, no obvious plateau is reached due to the formation of a lose network of crosslinks. All other materials ($Alg_{20mM\_4\,°C}$, $Alg_{12.5mM\_RT}$ and $Alg_{12.5mM\_4\,°C\_w/o\,stirring}$) show a markedly different, almost linear trend in the double-logarithmic plot. By comparing samples Alg_{0mM_RT}, $Alg_{5mM\_4\,°C}$, $Alg_{12.5mM\_4\,°C}$, $Alg_{20mM\_4\,°C}$ with increasing $CaCO_3$ contents, figure 3(a) clearly shows the increase in viscosity at low shear rates. At the lowest measured shear rate of 0.8 s^{-1}, a 100-fold increase in the viscosity can be achieved by pre-crosslinking. Due to the beneficial shear thinning behavior, the increase in viscosity at 1000 s^{-1} is only around three times. This

is a first indication that the performance of the inks is increased by the pre-crosslinking, due to high and shape preserving viscosities at rest, but low and more cell friendly viscosities at high shear rates. Moreover, a slope of close to minus one in the double logarithmic plot $\left(\frac{dlog(\eta)}{dlog(\dot{\gamma})} = -1\right)$ can be observed at low shear rates for samples $Alg_{12.5mM\_4\,°C}$, $Alg_{20mM\_4\,°C}$, $Alg_{12.5mM\_RT}$ and $Alg_{12.5mM\_4\,°C\_w/o\,stirring}$. This result indicates the presence of a yield point τ_y. In order to find the values for τ_y of the different inks, a simplified Ponslinki model was used to fit the graphs [44]:

$$\eta(\dot{\gamma}) = \frac{\tau_y}{\dot{\gamma}} + \eta_0 \left[1 + \left(\frac{\dot{\gamma}}{\dot{\gamma}_c}\right)^\alpha\right]^\beta \qquad (6)$$

Here, η_0 is the zero shear viscosity, $\dot{\gamma}_c$ the critical shear rate, α the transition control factor and β the exponent which can be described as:

$$\beta = \frac{n-1}{\alpha} \qquad (7)$$

with the power-law index n.

The resulting fit functions can be observed in the top right corner of figure 3(a). For the pure alginate solution without a yield point, τ_y was fixed to the value zero, resulting in a simplified Carreau-Yasuda model. For all other samples, τ_y was determined via the fitting function with the restriction that η_0 was fixed to the value of 1.44 Pas, which equals the zero shear viscosity of the non-crosslinked alginate solution. The yield points obtained are shown in the supplementary information (table 3 in the supplementary materials) in combination with the quality of the related fit function (R-Squared) and viscosities at a shear rate of 0.8 s^{-1}. The yield points indicate the presence of an increasingly strong network when

increasing the amount of $CaCO_3$ or the temperature, as well as when switching the processing conditions from stirring to non-stirring.

Considering figure 3(b), it can be observed that the non-crosslinked and weakly crosslinked samples (Alg_{0mM_RT}, $Alg_{5mM\_4\,°C}$), have a $\tan(\delta) > 1$ over the whole frequency range measured. This shows the dominance of the fluid-like behavior and thus it correlates well with the observation of an indicated plateau region of the weakly-crosslinked sample ($Alg_{5mM\_4\,°C}$) in figure 3(a). In comparison to that, all samples which show an almost linear trend in figure 3(a) also show a $\tan(\delta) < 1$ over the whole frequency range. Thus, these samples are dominated by their elastic behavior which indicates a stronger and denser crosslinking network.

Considering all these observations, the results show that pre-crosslinking with $CaCO_3$ and GDL has a strong influence on shear-dependent viscosity and leads to an increased network formation with increasing amounts of added calcium.

3.1.3. Shear stress, shear rate, velocity and residence time flow profiles

In this section, the rheological data of the bioinks including cells (according to section 2.6 In vitro studies) are analyzed. From the obtained parameters, an estimate of the velocity, shear rate, shear force and residence time profiles could be calculated for these bioinks which were also used for cell viability tests. When comparing the shear flow measurements with cells (figure 8—supplementary information) to those without cells, no substantial change in the trend of the curves can be observed. Slight changes in the viscosity values might occur due to the dilution of the hydrogel with DMEM or by the effect of cells acting as soft particle fillers.

In order to fit the graphs and create model functions, two different equations were chosen. On the one hand, for $Alg_{20mM\_4\,°C}$ where no plateau region at low shear rates was observed, a simple power-law model was used [45]:

$$\eta = K\dot{\gamma}^{n-1} \tag{8}$$

with the viscosity η, shear rate $\dot{\gamma}$, shear thinning coefficient K and exponent n. This model was chosen with the assumption of wall adhesion and real flow inside the tip channel. As the latter was revealed by preliminary flow experiments the power-law appeared as a simple model to estimate the flow properties of the pre-crosslinked ink. Although the appearance of wall slip is still to be examined, all following calculations were performed without taking it into account. The reason behind is that in the case of wall slip, the flow profile would result in a plug flow and thus highly reduced shear stresses on embedded cells. In the unfavorable scenario of wall adhesion, higher shear stresses will occur and thus it will be discussed in the following.

On the other hand, in the case of Alg_{0mM_RT} with a clearly visible plateau region, the Carreau-Yasuda model was chosen for fitting the function [44]:
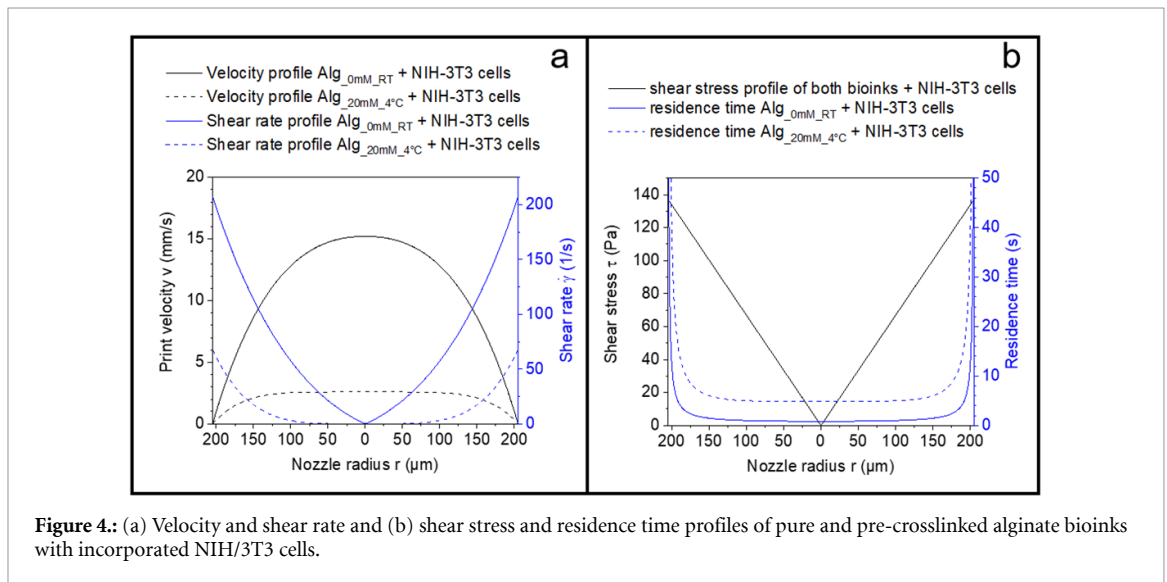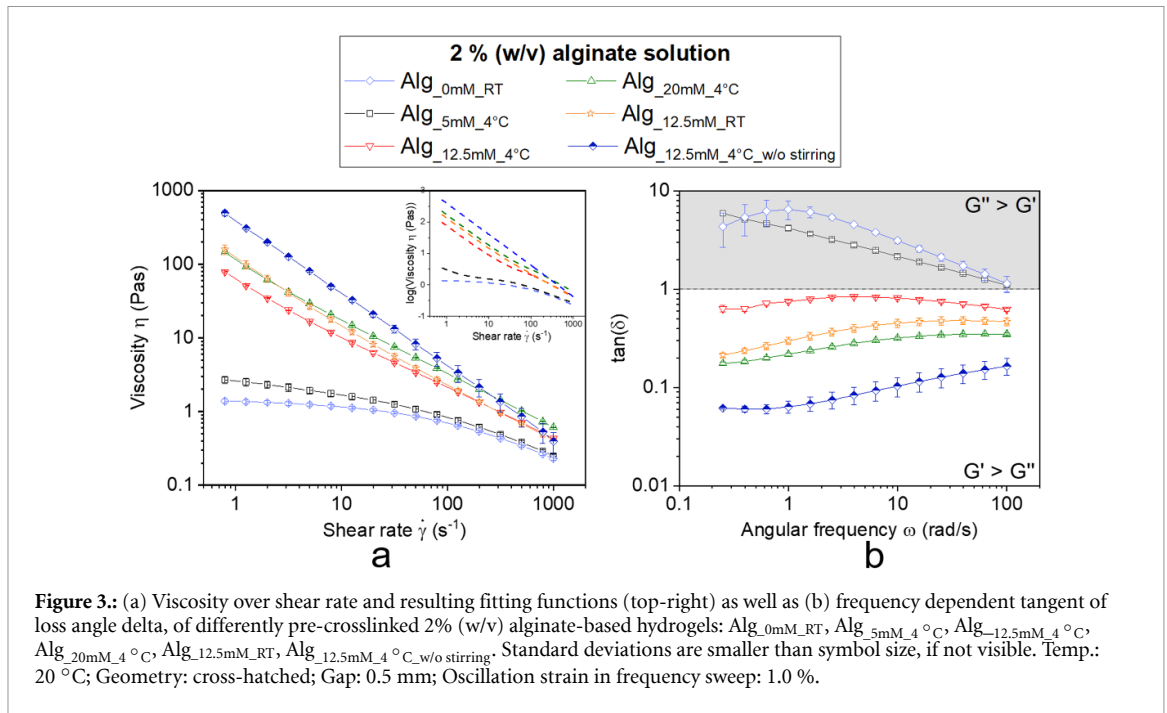
$$\eta(\dot{\gamma}) = \eta_\infty + (\eta_0 - \eta_\infty)\left[1 + \left(\frac{\dot{\gamma}}{\dot{\gamma}_c}\right)^a\right]^{\left(\frac{N-1}{a}\right)} \tag{9}$$

where η_0 is the zero shear and η_∞ the infinite shear viscosity, $\dot{\gamma}_c$ the critical shear rate, a the transition control factor and N the power-law index.

The resulting model functions and parameters when fitting with those equations can be found in section 5.2, supplementary information, which are necessary to calculate flow profiles from the rheological data. The profiles in figures 4(a) and (b) were calculated according to Paxton *et al* [30] in case of the pre-crosslinked alginate (Power-law model), or with a Python script provided by Müller *et al* in case of the pure alginate solution (Carreau-Yasuda model) [Müller *et al*—submitted in PLOS ONE—'Flow and hydrodynamic shear stress inside a printing needle during biofabrication']. These graphs depict a cross-section of the printing nozzle, where r = 0 μm represents the center of the nozzle and r = 205 μm represents the nozzle wall.

Figure 4(a) shows that the velocity of the pure alginate bioink is distinctly higher than that of the pre-crosslinked bioink. As the two bioinks were printed with the same pressure and nozzle, this behavior can simply be explained by the increased viscosity of the pre-crosslinked bioink. At the center of the nozzle, where the maximum velocity is reached, this results in values of 15.2 mm s^{-1} and 2.6 mm s^{-1} for non-crosslinked and pre-crosslinked bioink, respectively. Accordingly, the shear rate profiles of the non-crosslinked bioink shows higher values than the pre-crosslinked one.

However, the more important parameters in terms of cell damage and survival are given in figure 4(b). On the one hand, the shear stress profile is given which is, in the case of our model, only dependent on the die geometry and printing parameters, but not on the material properties themselves [30, 54]. It results in linearly increasing shear stresses from the center of the nozzle ($\tau = 0$ Pa), towards the wall, where a maximum value of $\tau = 137$ Pa is reached. On the other hand, the residence time which is dependent on the materials flow properties is shown in figure 4(b). Thus, the flow properties play a crucial role in how strong the cells will be damaged during printing, as they determine the residence time during which the cells are exposed to increased shear stresses. More precisely, it was shown before by Snyder *et al* [55] that apart from printing at higher stress intensity, also increased residence times lead to necrosis in a larger subpopulation of cells. Furthermore, they hypothesized that the increased number of necrotic cells might affect cell viability and differentiation of the local cell population [55]. Another study showed

Figure 3.: (a) Viscosity over shear rate and resulting fitting functions (top-right) as well as (b) frequency dependent tangent of loss angle delta, of differently pre-crosslinked 2% (w/v) alginate-based hydrogels: Alg_0mM_RT, Alg_5mM_4 °C, Alg_12.5mM_4 °C, Alg_20mM_4 °C, Alg_12.5mM_RT, Alg_12.5mM_4 °C_w/o stirring. Standard deviations are smaller than symbol size, if not visible. Temp.: 20 °C; Geometry: cross-hatched; Gap: 0.5 mm; Oscillation strain in frequency sweep: 1.0 %.

Figure 4.: (a) Velocity and shear rate and (b) shear stress and residence time profiles of pure and pre-crosslinked alginate bioinks with incorporated NIH/3T3 cells.

that shear stresses < 5 kPa in the nozzle hardly have any effect on the cell viability directly after printing resulting in an average cell viability of 96 %. In that paper, also alginate solutions (0.5, 1.0 and 1.5% (w/v)) were used for the experiments, in combination with L929 mouse fibroblasts [56]. When translating these previous observations to our results, a high cell viability after printing is expected for both materials due to very low maximum shear forces of around 0.14 kPa. The pre-crosslinked bioink would be more likely to damage the cells, as the average residence time of 9.6 s is around three-fold the residence time of the non-crosslinked bioink with an average residence time of 3.3 s. However, the cell viability after printing will be further discussed in section 3.4.

3.2. Printability and shrinkage

The following section serves to visualize the influence of pre-crosslinking on the rheological behavior (section 3.1 Rheology) and connect those values to the printability. Moreover, the shrinkage of different bioink formulations will be compared.

First of all, the printability values (P) and shrinkages ($\bar{S}$) calculated according to section 2.4, as well as the viscosity values from shear flow graphs at 0.8 s^{-1} for three selected bioinks, are given in table 2. Those bioinks were chosen as they represent one bioink which lacks printability due to low viscosity, one with good printability and one which lacks printability due to strong crosslinking.

It can be observed that the shrinkage of the scaffolds during post-crosslinking is reduced markedly

Table 2. Overview of shrinkage $\bar{S}$, printability P, viscosity η at a shear rate of 0.8 s^{-1} and tan(δ) for selected bioinks.

2% (w/v) alginate solution	Shrinkage $\bar{S}$ (%)	Printability P	Viscosity η (Pas) $\dot{\gamma} = 0.8$ s^{-1}	tan(δ) 1% strain; 10 rad s^{-1}
Alg$_{0mM\_RT}$	48.2 ± 3.3	0.646	1.4 ± 0.1	2.31 ± 0.03
Alg$_{20mM\_4\,°C}$	32.9 ± 5.6	0.953	146 ± 7	0.34 ± 0.02
Alg$_{12.5mM\_4\,°C\_w/o\,stirring}$	32.1 ± 0.1	0.898	492 ± 41	0.11 ± 0.00

by the pre-crosslinking. The pure alginate solution shows a shrinkage of almost 50% while the shrinkage of pre-crosslinked bioinks is reduced to around 32–33 %. This observation substantiates the hypothesis that physical Ca^{2+} crosslinks are present in the pre-crosslinked hydrogels. Thus, less new cross-links will be formed during the post-crosslinking process of the latter, leading to less shrinkage.

With respect to the printability values, it should be highlighted that, theoretically, printability can vary in the range 0 < P ≤ 1, but, practically, no values below 0.6 were measured. As the shear thinning behavior was already shown and discussed in section 3.1.2, table 2 only provides the viscosity of the bioinks at a shear rate of 0.8 s^{-1}, representing an estimate of the viscosity at rest. In addition, the loss angle tan(δ) is given, in order to show if either the elastic behavior (tan(δ) < 1) or the viscous behavior (tan(δ) > 1) of the material dominates. In conclusion, it can be shown that the viscosity as well as tan(δ) can be connected to the printability, indicating a window of good printability at a viscosity of around 150 Pas ($\dot{\gamma} = 0.8$ s^{-1}) and tan(δ) of 0.34 (1% strain, 10 rad s^{-1} frequency), which is in good accordance with the reported data and conclusion by Gao *et al* [57]. Moreover, the viscosity data and/or storage and loss moduli of Alg$_{20mM\_4\,°C}$ are comparable to these of other well printable alginate-based bioinks [58–61]. When under-gelation (Alg$_{0mM\_RT}$) or over-gelation (Alg$_{12.5mM\_4\,°C\_w/o\,stirring}$) occurs, the printability decreases due to either too low or too high viscosities at low shear rates, respectively. Moreover, the values of tan(δ) show that the flow property of pure alginate solution is dominated by viscous behavior, leading to viscous flow of the scaffold after printing. Contrary to this, the well printable bioink with 20 mM CaCO$_3$ pre-crosslinking is dominated by elastic behavior, indicated by a tan(δ) of 0.34. The elastic component (due to the formation of a network) leads to the ability of the material to store energy and thus, to an increased shape fidelity. However, when the network formation is too strong and insufficient viscous flow occurs in the bioink, the printability also decreases, which can be observed for sample Alg$_{12.5mM\_4\,°C\_w/o\,stirring}$. A similar and even more pronounced effect occurred when a comparison bioink, pre-crosslinked with CaCl$_2$ at the same concentrations, was supposed to be printed under similar conditions. For this purpose, a 4% (w/v) alginate

solution and a 40 mM CaCl$_2$ solution were prepared separately. Then, with a volume fraction of 1:1, CaCl$_2$ solution was added to the alginate solution dropwise at 4 °C and stirred for 48 h. Due to the rapid crosslinking, a strongly crosslinked alginate bulk, immersed in CaCl$_2$ solution, formed. This alginate hydrogel bulk could not be printed with a comparable nozzle, even at the maximum available pressure of 6 bar.

These results are further visualized in figure 5 which shows printed cuboids and parallel strands of the formulations given in table 2. The images illustrate the effect of pre-crosslinking on the printability. When looking at panels a and b, a lack of shape fidelity can be clearly observed for the pure alginate solution. The surface tension leads to the formation of a round shaped droplet in figure 5(a), although a cuboid was supposed to be printed. Moreover, in figure 5(b), the surface tension of the liquid also leads to droplet formation of the strands, which consequently merge. Thus, a very poor shape fidelity is given which matches with the dominating loss modulus (G") of this formulation. When inspecting figure 5(c), a cuboid structure with an almost exact side length of 15 mm can be perceived. Furthermore, figure 5(d) shows nicely aligned strands in horizontal direction, which do not merge or have any protrusions. Both of the latter figures show that the high value for printability P of 0.953 for this bioink is justified. With increasing viscosity and decreasing tan(δ) however, the printability drops down to 0.898. In figures 5(e) and (f), the decreased printability can clearly be observed. Due to the highly elasticity dominated property of this ink, the material behaves solid-like. Thus, during printing and undergoing high shear strains, the material rips apart unevenly which results in abrasive edges and inhomogeneous strands.

In order to further emphasize the printability and shape fidelity of the best printable bioink, figures 5(g)–(i) shows a variety of different perspectives and magnifications of bioink IV, which was well printable. In figures 5(g) and (h), a porous scaffold with 5 mm in height is shown. It can be observed that the pores reach through the whole height of the scaffold, speaking for good shape fidelity. However, no porosity in z-dimension could be observed. By further developing the method, especially investigating different methods of stirring for high viscosity materials, it is assumed that rheological properties can further be improved, which might even lead to z-dimensional
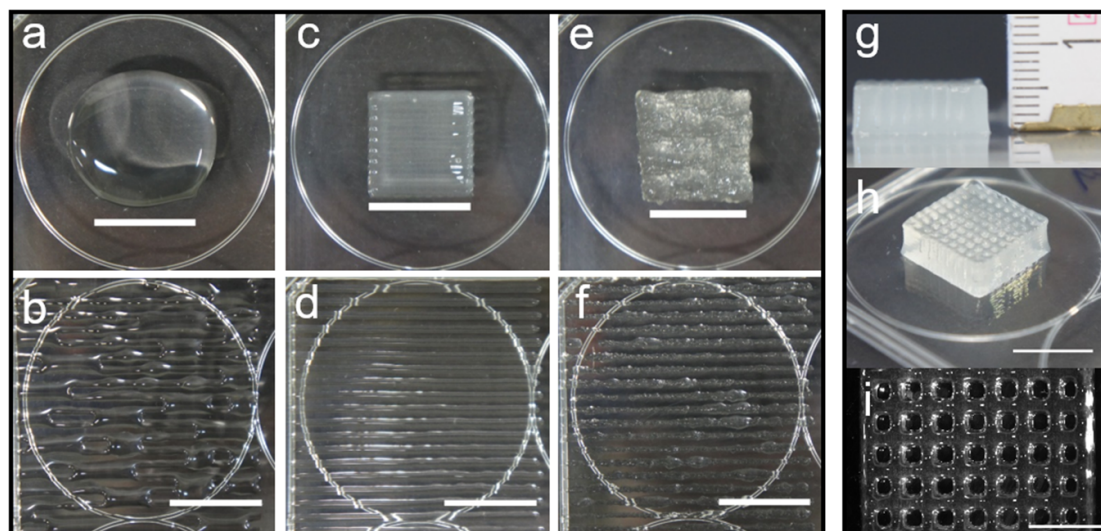
Figure 5. Illustration of the effect of pre-crosslinking on the printability of alginate. a/c/e: printed cuboids with 15 mm side length; b/d/f: struts printed with a gap distance of 2.1 mm from center to center. a/b were printed with Alg_{0mM_RT}, c/d with $Alg_{20mM\_4\,^\circ C}$ and e/f with $Alg_{12.5mM\_4\,^\circ C\_w/o\ stirring}$. Scale bars: 15 mm. g/h/i: Different perspectives and magnifications of 3D printed porous structures, using $Alg_{20mM\_4\,^\circ C}$. Scale bar h: 15 mm, i: 5 mm.

porosity. The microscopy image in figure 5(i), shows the pore structure of such scaffolds from a top view. With those images, an average pore size of 1.10 mm and strut width of 0.74 mm could be determined. Although the 3D structure looks promising, the pores show slightly rounded edges and the ones on the extreme edge of the scaffolds are smaller in size, which might be an artefact of the printer.

3.3. Mechanical properties of post-crosslinked matrix materials

A crucial factor for cell viability and differentiation is given by the mechanical properties of the matrix wherein the cells are embedded. As shown by Huebsch *et al* [62], stem cells do not only sense, but also respond to the mechanical properties of their surrounding extracellular matrix. However, it is also important to control the Young's Modulus of the matrix that is used to embed fully differentiated cells.

In figure 6, the Young's moduli of the two material compositions which were also used for cell viability tests are given. Although the concentration of alginate inside the hydrogel and the $CaCl_2$ concentration for post-crosslinking were the same, significantly different values can be observed. The Young's modulus of pure alginate hydrogels with 17.7 kPa is significantly higher (more than two times) than that of the pre-crosslinked hydrogels with 7.3 kPa.
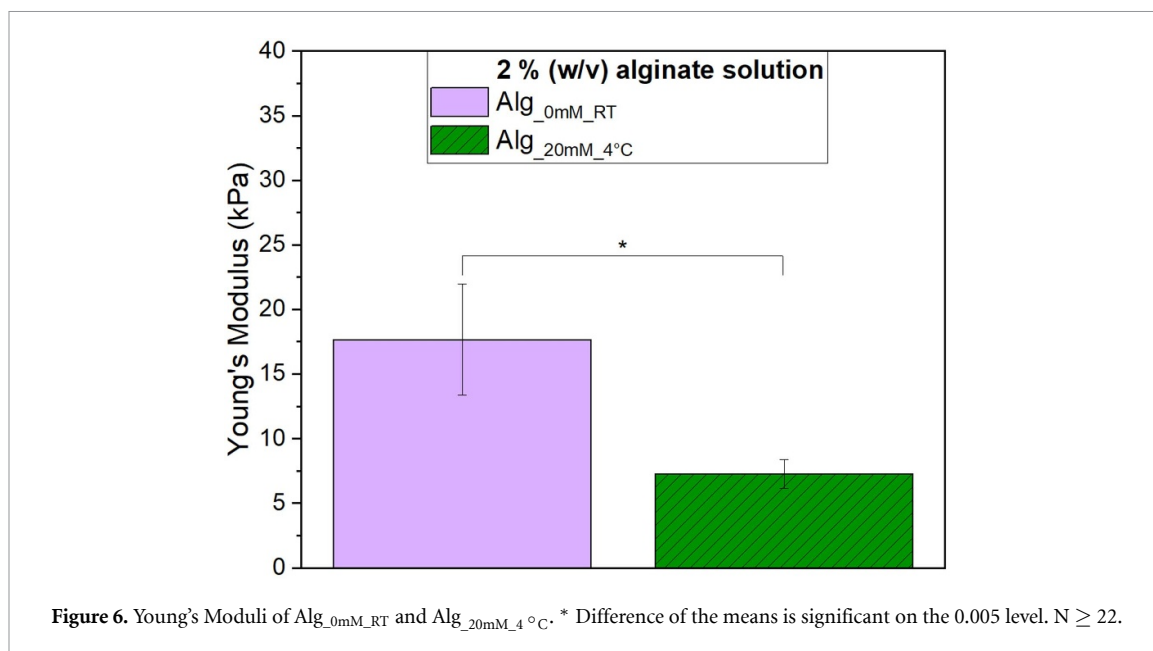
So far, this reduction cannot be explained with certainty. However, even if a relatively high calcium concentration of around 20 mM is already present inside the pre-crosslinked hydrogel, the formation of an overall 3D network was hindered due to stirring. As the particle current density and thus the diffusion rate are dependent on the concentration gradient (Fick's law), one hypothesis is that less calcium ions

interpenetrate the pre-crosslinked hydrogels during the post-crosslinking time of ten minutes. In order to gain the same Young's moduli for both materials, preliminary results showed that longer post-crosslinking durations are necesarry. Apart from the reduced diffusion rate, the different stiffness could also be caused by the fact that many crosslinks have already been formed inside the pre-crosslinked hydrogel, which reduces the mobility of alginate chains. Thus, the process of forming new crosslinks might be extended. When comparing the obtained values with data reported by Liu *et al* [63], it turns out that the Young's modulus of our material is comparable to a range of soft tissues like spleen, skin or muscles.

3.4. Cell viability and morphology post-printing

The aim of this part of the study was to investigate the influence of printing with either pure alginate solution or pre-crosslinked alginate on the viability of NIH/3T3 murine fibroblast cells. The cell tests were conducted according to section 2.6. Similar and homogeneous cell distributions were observed visually for both materials during 2D imaging of the constructs, confirming a homogenous cell distribution inside the bioink owing to the mixing procedure.

Live and dead stainings, as well as light microscopy images were captured after 1 d, 3 d, 7 d and 14 d after printing. These images showed roundly shaped cell morphology for cells embedded in pure alginate hydrogels over the whole period of time. Moreover, the vast majority of cells were separated from each other and did not show agglomerates on day one and three of cell culture. After seven days of cell culture, the cell spots showed an increased diameter, which was even more pronounced after 14 d. This might be a sign of proliferating cells which are not able to

Figure 6. Young's Moduli of Alg$_{0mM\_RT}$ and Alg$_{20mM\_4\,^\circ C}$. * Difference of the means is significant on the 0.005 level. N $\geq$ 22.
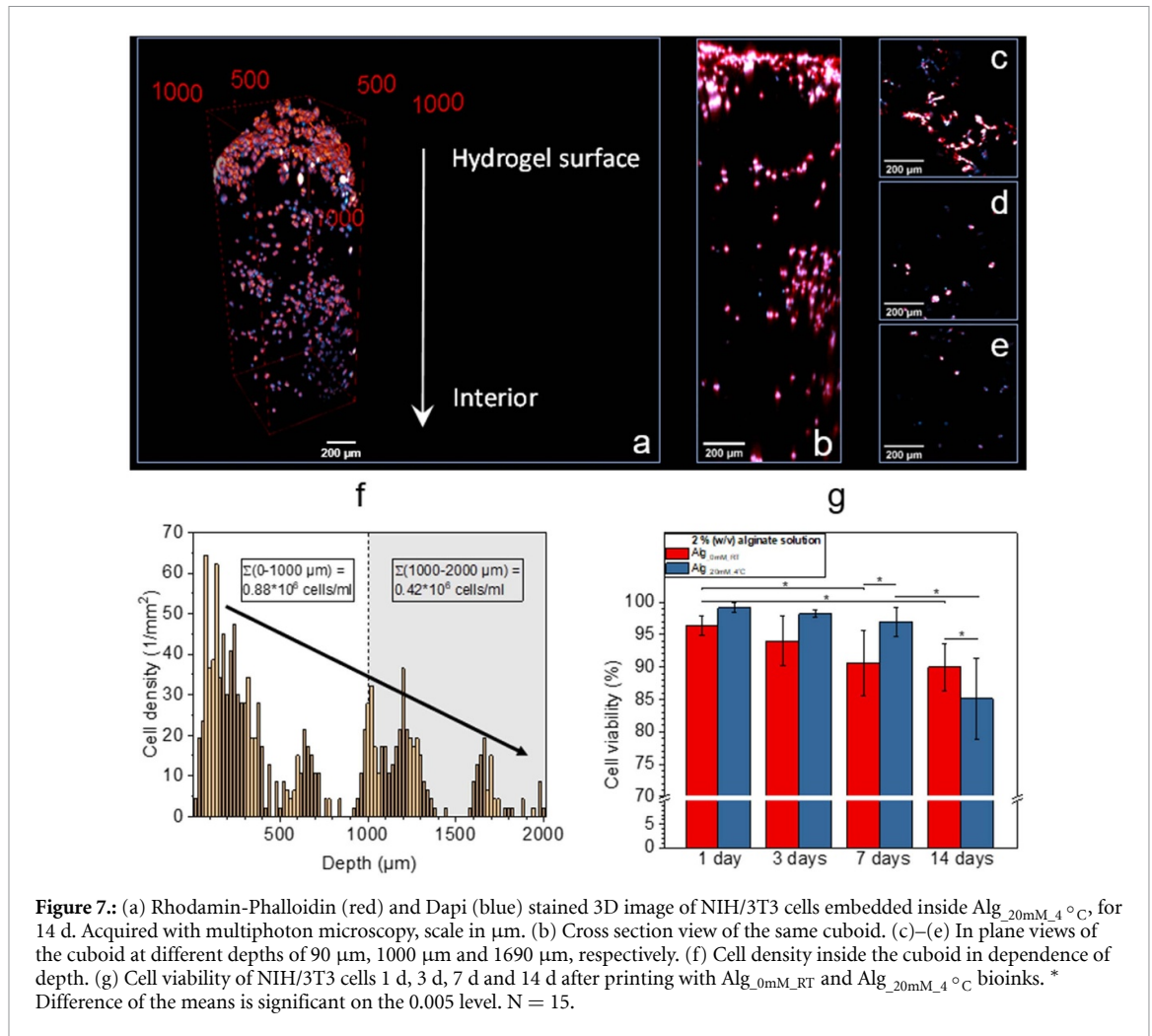
grow through the hydrogel, either due to an excessive stiffness of the surrounding material, a lack of cell-adhesive moieties in the material, or a combination of both. In general, this observation was expected and is in agreement with literature, as native alginate is a bioinert material which does not have any binding sites where cells can directly attach to [64]. Moreover, unmodified alginate is known to show slow degradation rates and thus, will maintain its initial stiffness over long periods of time [65, 66].

In cell culture of pre-crosslinked alginate samples, the same observation was made on day one and three in 2D bright field imaging. However, after 7 and 14 d, the morphology of cells started to be more elongated and agglomerates could be observed. Due to this rather unexpected behavior, 3D images with cell nucleus and actin-filament staining were captured with a multi-photon microscope. Figure 7(a) shows such a 3D stack of cells embedded inside the pre-crosslinked hydrogel sample, after 14 d of cell culture. The very top of the image displays the hydrogel surface, whereas everything below that shows the interior of the hydrogel. It can be observed that the hydrogel surface is covered with many cells compared to the interior. This observation is further highlighted in figures 7(b)–(e). Figure 7(b) shows a vertical cross section view of the 3D stack, whereas figures 7(c)–(e) shows horizontal cross sections at depths of 90 μm, 1000 μm and 1690 μm. Those images reveal that the cells on the surface show an interconnected actin-filament network. In contrast to that, the cells which are situated 1000 μm or deeper inside the hydrogel are separated from each other and no actin-filaments can be observed between the cell nuclei. Thus, one can conclude that the observations of cell spreading made in 2D were surface-related effects. Those effects might have occurred in the pre-crosslinked hydrogels

but not in the pure alginate hydrogels due to the reduced stiffness (section 3.3). Embedded in less stiff hydrogels, cells would have the possibility to move through the hydrogel. Especially close to the surface, cells have very good supply of nutrition and on the surface itself also the opportunity to reach out easily to each other to form spread structures as observed in figure 7(c). Moreover, the cell density in dependence of the depth is shown in figure 7(f) and clarifies the trend of fewer cells in the depth of the structure ($0.42*10^6$ cells ml^{-1}) compared to the surface ($0.88*10^6$ cells ml^{-1}). Interestingly, when comparing the counted cell density to the initial cell density ($1.0*10^6$ cells ml^{-1}), it becomes apparent that fewer cells were counted inside the construct. Conceivable hypotheses to explain this observation could be that either the cells were not evenly distributed in the first place, or that the counting based on image data is not capable to separate cell nuclei which lie close to each other in cell agglomerates.

In addition, cell viability was considered. Figure 7(g) shows the percentage of living cells compared to dead cells for the pure as well as for the pre-crosslinked alginate hydrogel after 1 d, 3 d, 7 d and 14 d. Figure 7(g) shows that the mean cell viability for both tested materials is above 90% over a period of seven days. Apart from this, the cell viability in pre-crosslinked alginate exceeds the one in pure alginate during this time period. Significant differences between the samples on the 0.05 level were found between 1 d and 7 d as well as 1 d and 14 d samples in non-crosslinked alginate bioink, as well as between 7 d and 14 d in pre-crosslinked alginate. The strong decrease of cell viability between 7 d and 14 d of the pre-crosslinked samples is assumed to be due to a slightly misleading read out of counting live and dead cells. As discussed before, especially after 14 d of cell

Figure 7.: (a) Rhodamin-Phalloidin (red) and Dapi (blue) stained 3D image of NIH/3T3 cells embedded inside $Alg_{20mM\_4\,°C}$, for 14 d. Acquired with multiphoton microscopy, scale in µm. (b) Cross section view of the same cuboid. (c)–(e) In plane views of the cuboid at different depths of 90 µm, 1000 µm and 1690 µm, respectively. (f) Cell density inside the cuboid in dependence of depth. (g) Cell viability of NIH/3T3 cells 1 d, 3 d, 7 d and 14 d after printing with Alg_{0mM_RT} and $Alg_{20mM\_4\,°C}$ bioinks. * Difference of the means is significant on the 0.005 level. N = 15.

culture in pre-crosslinked hydrogel, the cells started to spread significantly. Thus, it was not possible to separate living cells in ImageJ software with absolute certainty, possibly leading to a lower number of detections than actual living cells inside the hydrogels. In general, a trend for decreasing cell viability over time can be noticed which is not questioned, as the adhesive fibroblast cells do not have any cell-adhesive moieties to attach to. In order to incorporate cell adhesive motifs, native alginate can be chemically modified with RGD-sequences [67, 68] or with proteins containing such motifs [69, 70]. Although the rheological properties are most likely to change by any type of modification, it is assumed that the universal pre-crosslinking technique could help to increase the printability of other alginate-based hydrogels, too.

However, the main goal of this experiment was to determine whether the pre-crosslinking of alginate has an influence on the cell viability after printing. Due to the fact that the mean value of cell viability in pre-crosslinked alginate exceeds the one in pure alginate throughout the first week, it can be concluded that the pre-crosslinking process itself, as well as different residence times during printing, did not harm the cells. Consequently, NIH/3T3 cells were not

affected by the increased viscosity, nor the decreased pH values which they were exposed to for a short period of time.

4. Conclusions

Advanced bioinks for biofabrication need to fulfil a variety of material properties and requirements. Hence, this study addressed a range of those properties, such as shear thinning behavior, shape fidelity and cell viability of different bioinks.

From a rheological point of view, the transition from a solution to a crosslinked hydrogel could be shown, also revealing different kinetics at room temperature and at 4 °C. The increasing viscosity at low shear rates due to pre-crosslinking can therefore be clearly ascribed to the network formation, whereas particle reinforcement due to undissolved $CaCO_3$ or precipitated calcium phosphate particulates is very unlikely. Moreover, all tested bioinks showed shear thinning behavior which is very advantageous in terms of 3D bioprinting, as cells will 'suffer' less from long residence times under high shear stress conditions [30]. Rheological key parameters, namely the viscosity (at $\dot{\gamma} = 0.8$ s^{-1}), tan(δ) (at 1% strain;

10 rad s^{-1}), the yield stress τ_y and the shear thinning coefficient n, could be linked to the printability of printed cuboid structures. It was ascertained that the alginate based bioinks were best printable with a viscosity of around 150 Pas ($\dot{\gamma} = 0.8$ s^{-1}), tan(δ) of 0.34 (1% strain; 10 rad s^{-1}), yield stress of 170 Pa and shear thinning coefficient $n = 0.23$. For extrusion-based bioprinting of pre-crosslinked alginate, those values lie close to the optimum. These beneficial printing properties were achieved by pre-crosslinking with a molar concentration of 20 mM CaCO$_3$ while constantly stirring the bioink, in order to have a homogeneous distribution of CaCO$_3$ particles and to preserve the viscous behavior of the bioink. On the contrary, it was not possible to print a comparison bioink pre-crosslinked with CaCl$_2$ (instead of CaCO$_3$), even using the same salt concentrations.

Furthermore, rheological flow-sweep graphs could be used to estimate shear force, shear rate, residence time and velocity profiles in the nozzle. However, it is important to keep in mind that all calculations performed to generate the different profiles are based on the assumption of linear, steady flow and no slip between bioink and nozzle wall. In case of predominant yield stresses and resulting plug flow, the stress on cells would be reduced markedly. Thus, the absolute values should be used with caution, and they show the least favorable case in terms of stresses affecting the cells. The power-law model is restricted to describe the measured region of shear rates. As it is only an empiric model without underlying physical theory, it cannot describe the low-shear and high-shear rate constant viscosity data. Nevertheless, considering the cell viability studies, it could be proven that the increased residence time at the same pressure does not negatively affect the cell viability when pre-crosslinking the alginate. Moreover, the pre-crosslinking procedure and all components do not significantly affect viability of NIH/3T3 cells in a negative manner over a period of seven days.

Hence, the pre-crosslinking technique used in this paper was proven to be suitable for significantly enhancing the printability of alginate based bioinks without losses in the viability of NIH/3T3 cells. Thus, this technique comprises the possibility to improve the printability of alginate based bioinks in general and is therefore extremely useful in the field of biofabrication.

Acknowledgments

ORCID iD

Jonas Hazur ⬤ https://orcid.org/0000-0002-3370-0666

References

[1] Reakasame S and Boccaccini A R 2018 Oxidized alginate-based hydrogels for tissue engineering applications: a review *Biomacromolecules* **19** 3–21

[2] Annabi N, *et al* 2014 25th anniversary article: rational design and applications of hydrogels in regenerative medicine *Adv. Mater.* **26** 85–124

[3] Pawar S N and Edgar K J 2012 Alginate derivatization: a review of chemistry, properties and applications *Biomaterials* **33** 3279–305

[4] Boontheekul T, Kong H-J and Mooney D J 2005 Controlling alginate gel degradation utilizing partial oxidation and bimodal molecular weight distribution *Biomaterials* **26** 2455–65

[5] Mørch Y A, Donati I, Strand B L and Skjåk-Bræk G 2006 Effect of Ca2+, Ba2+, and Sr2+ on alginate microbeads *Biomacromolecules* **7** 1471–80

[6] Kong H-J, Lee K Y and Mooney D J 2002 Decoupling the dependence of rheological/mechanical properties of hydrogels from solids concentration *Polymer* **43** 6239–46

[7] Draget K I, Simensen M K, Onsyen E and Smidsrød O 1993 Gel strength of Ca-limited alginate gels made in situ *Hydrobiologia* **260–1** 563–5

[8] Chan E-S, Lim T-K, Voo W-P, Pogaku R, Tey B T and Zhang Z 2011 Effect of formulation of alginate beads on their mechanical behavior and stiffness *Particuology* **9** 228–34

[9] Kaygusuz H, Evingür G A, Pekcan Ö, von Klitzing R and Erim F B 2016 Surfactant and metal ion effects on the mechanical properties of alginate hydrogels *Int. J. Biol. Macromol.* **92** 220–4

[10] Stößlein S, Grunwald I, Stelten J and Hartwig A 2019 In-situ determination of time-dependent alginate-hydrogel formation by mechanical texture analysis *Carbohydr. Polym.* **205** 287–94

[11] Voo W-P, Ooi C-W, Islam A, Tey B-T and Chan E-S 2016 Calcium alginate hydrogel beads with high stiffness and extended dissolution behaviour *Eur. Polym. J.* **75** 343–53

[12] Yeung R A and Kennedy R A 2019 A comparison of selected physico-chemical properties of calcium alginate fibers produced using two different types of sodium alginate *J. Mech. Behav. Biomed. Mater.* **90** 155–64

[13] Hölzl K, Lin S, Tytgat L, Van Vlierberghe S, Gu L and Ovsianikov A 2016 Bioink properties before, during and after 3D bioprinting *Biofabrication* **8** 32002

[14] Detsch R, Sarker B, Zehnder T, Boccaccini A R and Douglas T E L 2014 Additive manufacturing of cell-loaded alginate enriched with alkaline phosphatase for bone tissue engineering application *BioNanoMater.* **15** 3–4

[15] Li H, Tan C and Li L 2018 Review of 3D printable hydrogels and constructs *Mater. Des.* **159** 20–38

[16] Berg J *et al* 2018 Optimization of cell-laden bioinks for 3D bioprinting and efficient infection with influenza A virus *Sci. Rep.* **8** 13877

[17] Li Z, Huang S, Liu Y, Yao B, Hu T, Shi H, Xie J and Fu X 2018 Tuning alginate-gelatin bioink properties by varying solvent and their impact on stem cell behavior *Sci. Rep.* **8** 8020

[18] Leite Á J, Sarker B, Zehnder T, Silva R, Mano J F and Boccaccini A R 2016 Bioplotting of a bioactive alginate dialdehyde-gelatin composite hydrogel containing bioactive glass nanoparticles *Biofabrication* **8** 35005

[19] Ivanovska J, Zehnder T, Lennert P, Sarker B, Boccaccini A R, Hartmann A, Schneider-Stock R and Detsch R 2016 Biofabrication of 3D alginate-based hydrogel for cancer research: comparison of cell spreading, viability, and adhesion characteristics of colorectal HCT116 tumor cells *Tissue Eng. C: Methods* **22** 708–15

[20] Izadifar M, Chapman D, Babyn P, Chen X and Kelly M E 2018 UV-assisted 3D bioprinting of nanoreinforced hybrid cardiac patch for myocardial tissue engineering *Tissue Eng. C: Methods* **24** 74–88

[21] Daly A C, Critchley S E, Rencsok E M and Kelly D J 2016 A comparison of different bioinks for 3D bioprinting of fibrocartilage and hyaline cartilage *Biofabrication* **8** 45002

[22] Narayanan L K, Huebner P, Fisher M B, Spang J T, Starly B and Shirwaiker R A 2016 3D-bioprinting of polylactic acid (PLA) nanofiber–alginate hydrogel bioink containing human adipose-derived stem cells *ACS Biomater. Sci. Eng.* **2** 1732–42

[23] Yildirim E D, Yin X, Nair K and Sun W 2008 Fabrication, characterization, and biocompatibility of single-walled carbon nanotube-reinforced alginate composite scaffolds manufactured using freeform fabrication technique *J. Biomed. Mater. Res. B: Appl. Biomater.* **87** 406–14

[24] Zehnder T *et al* 2016 Fabrication of cell-loaded two-phase 3D constructs for tissue engineering *Materials* **9** 887

[25] Ruther F, Distler T, Boccaccini A R and Detsch R 2018 Biofabrication of vessel-like structures with alginate di-aldehyde-gelatin (ADA-GEL) bioink *J. Mater. Sci. Mater. Med.* **30** 8

[26] Baker B M and Chen C S 2012 Deconstructing the third dimension: how 3D culture microenvironments alter cellular cues *J. Cell. Sci.* **125** 3015–24

[27] Grassi M, Sandolo C, Perin D, Coviello T, Lapasin R and Grassi G 2009 Structural characterization of calcium alginate matrices by means of mechanical and release tests *Molecules* **14** 3003–17

[28] Ramanujan S, Pluen A, McKee T D, Brown E B, Boucher Y and Jain R K 2002 Diffusion and convection in collagen gels: implications for transport in the tumor interstitium *Biohys. J.* **83** 1650–60

[29] Marchioli G *et al* 2015 Fabrication of three-dimensional bioplotted hydrogel scaffolds for islets of Langerhans transplantation *Biofabrication* **7** 25009

[30] Paxton N, Smolan W, Böck T, Melchels F, Groll J and Jungst T 2017 Proposal to assess printability of bioinks for extrusion-based bioprinting and evaluation of rheological properties governing bioprintability *Biofabrication* **9** 44107

[31] Skjak-Braek G, Grasdalen H and Smidsrod O 1989 lnhomogeneous polysaccharide ionic gels *Carbohydr. Polym.* **10** 31–54

[32] Chung J H Y, Naficy S, Yue Z, Kapsa R, Quigley A, Moulton S E and Wallace G G 2013 Bio-ink properties and printability for extrusion printing living cells *Biomater. Sci.* **1** 763

[33] Donati I, Holtan S, Mørch Y A, Borgogna M and Dentini M 2005 New hypothesis on the role of alternating sequences in calcium-alginate gels *Biomacromolecules* **6** 1031–40

[34] Nunamaker E A, Purcell E K and Kipke D R 2007 In vivo stability and biocompatibility of implanted calcium alginate disks *J. Biomed. Mater. Res.* A **83** 1128–37

[35] Liu X D, Bao D C, Xue W M, Xiong Y, Yu W T, Yu X J, Ma X J and Yuan Q 2003 Preparation of uniform calcium alginate gel beads by membrane emulsification coupled with internal gelation *J. Appl. Polym. Sci.* **87** 848–52

[36] Jensen H M, Larsen F H and Engelsen S B 2015 Characterization of alginates by nuclear magnetic resonance (NMR) and vibrational spectroscopy (IR, NIR, Raman) in combination with chemometrics *Methods Mol. Biol.* **1308** 347–63

[37] Grasdalen H 1983 High-field, 1H-n.m.r. spectroscopy of alginate: sequential structure and linkage conformations *Carbohydr. Res.* **118** 255–60

[38] McKee D, Thoma A, Bailey K and Fish J 2014 A review of hydrofluoric acid burn management *Plastic Surgery* **22** 95–98

[39] Smiths Medical ASD Data sheet Renacidin: (Citric acid, Glucono delt-lactone, and magnesium carbonate) Irrigation Solution (https://www.accessdata.fda.gov/drugsatfda_docs/label/2015/019481s013lbl.pdf)

[40] Liu X D, Yu W W Y, Zhang Y, Xue W M, Yu W T, Xiong Y, Ma X J, Chen Y and Yuan Q 2002 Characterization of structure and diffusion behaviour of Ca-alginate beads prepared with external or internal calcium sources *J. Microencapsul.* **19** 775–82

[41] Parke S A, Birch G G, MacDougall D B and Stevens D A 1997 Tastes, structure and solution properties of D-glucono-1,5-lactone *Chem. Senses* **22** 53–65

[42] Redey S A, Razzouk S, Rey C, Bernache-Assollant D, Leroy G, Nardin M and Cournot G 1999 Osteoclast adhesion and activity on synthetic hydroxyapatite, carbonated hydroxyapatite, and natural calcium carbonate: relationship to surface energies *J. Biomed. Mater. Res.* **45** 140–7

[43] Petite H, Viateau V, Bensaïd W, Meunier A, de Pollak C, Bourguignon M, Oudina K, Sedel L and Guillemin G 2000 Tissue-engineered bone regeneration *Nat. Biotechnol.* **18** 959–63

[44] Lapasin R and Pricl S 1995 *Rheology of Industrial Polysaccharides: Theory and Applications* (Boston, MA: Springer)

[45] Rao M A 2007 *Rheology of Fluid and Semisolid Foods: Principles and Applications* (Boston, MA: Springer) (https://doi.org/1010.1007/978-0-387-70930-7)

[46] Chimene D, Kaunas R and Gaharwar A K 2020 Hydrogel bioink reinforcement for additive manufacturing: a focused review of emerging strategies *Adv. Mater.* **32** e1902026

[47] Deo K A, Singh K A, Peak C W, Alge D L and Gaharwar A K 2020 Bioprinting 101: design, fabrication, and evaluation of cell-laden 3D bioprinted scaffolds *Tissue Eng.* A **26** 318–38

[48] Schindelin J *et al* 2012 Fiji: an open-source platform for biological-image analysis *Nat. Methods* **9** 676–82

[49] Oliver W C and Pharr G M 2004 Measurement of hardness and elastic modulus by instrumented indentation: advances in understanding and refinements to methodology *J. Mater. Res.* **19** 3–20

[50] Schneidereit D, Nübler S, Prölß G, Reischl B, Schürmann S, Müller O J and Friedrich O 2018 Optical prediction of single muscle fiber force production using a combined biomechatronics and second harmonic generation imaging approach *Light, Sci. Appl.* **7** 79

[51] Kruse C R, Singh M, Targosinski S, Sinha I, Sørensen J A, Eriksson E and Nuutila K 2017 The effect of pH on cell viability, cell migration, cell proliferation, wound closure, and wound reepithelialization: in vitro and in vivo study *Wound Repair Regen.* **25** 260–9

[52] Lee G-H, Hwang J-D, Choi J-Y, Park H-J, Cho J-Y, Kim K-W, Chae H-J and Kim H-R 2011 An acidic pH environment increases cell death and pro-inflammatory cytokine release in osteoblasts: the involvement of BAX inhibitor-1 *Int. J. Biochem. Cell Biol.* **43** 1305–17

[53] Walter B L, Pelteret J-P, Kaschta J, Schubert D W and Steinmann P 2017 On the wall slip phenomenon of elastomers in oscillatory shear measurements using parallel-plate rotational rheometry: I. Detecting wall slip *Polym Test* **61** 430–40

[54] Suntornnond R, Tan E, An J and Chua C 2016 A mathematical model on the resolution of extrusion bioprinting for the development of new bioinks *Materials* **9** 756

[55] Snyder J, Rin Son A, Hamid Q, Wang C, Lui Y and Sun W 2015 Mesenchymal stem cell printing and process regulated cell properties *Biofabrication* **7** 44106

[56] Blaeser A, Duarte Campos D F, Puster U, Richtering W, Stevens M M and Fischer H 2016 Controlling shear stress in 3D bioprinting is a key factor to balance printing resolution and stem cell integrity *Adv. Healthc. Mater.* **5** 326–33

[57] Gao T, Gillispie G J, Copus J S, Pr A K, Seol Y-J, Atala A, Yoo J J and Lee S J 2018 Optimization of gelatin-alginate composite bioink printability using rheological parameters: a systematic approach *Biofabrication* **10** 34106

[58] Cooper M H H G and Bartolo P J D S 2019 Development and characterisation of a photocurable alginate bioink for 3D bioprinting *Int. J. Bioprint.* **5** 12

[59] Jessop Z M, Al-Sabah A, Gao N, Kyle S, Thomas B, Badiei N, Hawkins K and Whitaker I S 2019 Printability of pulp

derived crystal, fibril and blend nanocellulose-alginate bioinks for extrusion 3D bioprinting *Biofabrication* **11** 45006

[60] Kim M H, Lee Y W, Jung W-K, Oh J and Nam S Y 2019 Enhanced rheological behaviors of alginate hydrogels with carrageenan for extrusion-based bioprinting *J. Mech. Behav. Biomed. Mater.* **98** 187–94

[61] López-Marcial G R, Zeng A Y, Osuna C, Dennis J, García J M and O'Connell G D 2018 Agarose-based hydrogels as suitable bioprinting materials for tissue engineering *ACS Biomater. Sci. Eng.* **4** 3610–6

[62] Huebsch N, Arany P R, Mao A S, Shvartsman D, Ali O A, Bencherif S A, Rivera-Feliciano J and Mooney D J 2010 Harnessing traction-mediated manipulation of the cell/matrix interface to control stem-cell fate *Nat. Mater.* **9** 518–26

[63] Liu J, Zheng H, Poh P S P, Machens H-G and Schilling A 2015 Hydrogels for engineering of perfusable vascular networks *Int. J. Mol. Sci.* **16** 15997–6016

[64] Jia J *et al* 2014 Engineering alginate as bioink for bioprinting *Acta Biomater* **10** 4323–31

[65] Bouhadir K H, Lee K Y, Alsberg E, Damm K L, Anderson K W and Mooney D J 2001 Degradation of partially oxidized alginate and its potential application for tissue engineering *Biotechnol. Prog.* **17** 945–50

[66] Lee K Y and Mooney D J 2012 Alginate: properties and biomedical applications *Prog. Polym. Sci.* **37** 106–26

[67] Rowley J A, Madlambayan G and Mooney D J 1999 Alginate hydrogels as synthetic extracellular matrix materials *Biomaterials* **20** 45–53

[68] Ho S S, Murphy K C, Binder B Y K, Vissers C B and Leach J K 2016 Increased survival and function of mesenchymal stem cell spheroids entrapped in instructive alginate hydrogels *Stem. Cells Transl. Med.* **5** 773–81

[69] Rastogi P and Kandasubramanian B 2019 Review of alginate-based hydrogel bioprinting for application in tissue engineering *Biofabrication* **11** 42001

[70] Wu Z, Li Q, Xie S, Shan X and Cai Z 2020 In vitro and in vivo biocompatibility evaluation of a 3D bioprinted gelatin-sodium alginate/rat Schwann-cell scaffold *Mater. Sci. Eng. C: Mater. Biol. Appl.* **109** 110530